EES Batteries

ROYAL SOCIETY
OF **CHEMISTRY**

PAPER
Lili Liu, Tao Wang, Yuping Wu *et al.*
Li$_{0.95}$Na$_{0.05}$FePO$_4$ as a trifunctional additive to boost the electrochemical performance of cathodes in lithium–sulfur batteries

Check for updates

Li$_{0.95}$Na$_{0.05}$FePO$_4$ as a trifunctional additive to boost the electrochemical performance of cathodes in lithium–sulfur batteries

Shuang Xia,†[a] Luo Yan,†[b] Nan Wang,[a] Qi Zhou,[a] Lili Liu, [ID] *[c] Bohao Peng,[a] Tao Wang, [ID] *[a] Faxing Wang, [ID] [a] Jiarui He,[a] Yuan Ma[a] and Yuping Wu [ID] *[a]

Lithium–sulfur batteries (LSBs) are regarded as some of the effective candidates for next-generation energy storage systems due to their high energy density. Conventional sulfur cathodes suffer from inadequate polysulfide adsorption and catalytic conversion capabilities, along with sluggish ion kinetics, leading to low utilization of active sulfur substances. These limitations hinder the practical application of LSBs. Here, micrometer-sized LNFP (Li$_{0.95}$Na$_{0.05}$FePO$_4$) with enhanced ion conductivity is innovatively proposed as an additive for the cathode to address this challenge. Through theoretical analysis (density functional theory, DFT) and empirical experiments, it is found that Na$^+$ doping not only exposes effective adsorption sites but also alters the electronic environment of Fe^{2+}/Fe^{3+}, thereby enhancing the adsorption and catalytic conversion abilities of LFP towards polysulfides. The multifunctional LNFP additive contributes to high performance for S cathodes. As a result, the assembled LSB with the LNFP additive delivers an initial discharge specific capacity of 953 mAh g^{-1} at 1 C and exhibits excellent cycling performance with a capacity decay of only 0.039% per cycle after 700 cycles. The prepared LSB retains a specific discharge capacity of 548 mAh g^{-1} after 300 cycles at 5 C. The LSB demonstrates a discharge specific capacity of 880 mAh g^{-1} under a high sulfur loading of 4.5 mg cm^{-2}. This work opens up new avenues for optimizing the performance of LSBs.

Broader context

Lithium–sulfur batteries (LSBs) are regarded as leading candidates for next-generation energy-efficient vehicles due to their high theoretical energy density. However, conventional sulfur cathodes suffer from insufficient adsorption of polysulfide intermediates and poor catalytic conversion, leading to low utilization efficiency of active sulfur substances. Moreover, the thickness of sulfur cathodes can reach tens of micrometers, and the insulating nature of elemental sulfur hinders the effective movement of electrons and Li$^+$ ions. We initially propose micron-sized Li$_{0.95}$Na$_{0.05}$FePO$_4$ (LNFP), a Na$^+$-doped LFP derivative with enhanced ionic conductivity, as a cathode additive to address these challenges. Our studies reveal that Na$^+$ doping effectively exposes more adsorption sites in LFP and enhances polysulfide adsorption via polythionate complex formation, with complete desorption achievable during redox cycling. Simultaneously, Na$^+$ doping alters the electronic environment of Fe^{2+}/Fe^{3+}, thereby boosting the inherent electronic conductivity of LFP. Consequently, this enables LNFP to convert adsorbed polysulfides into sulfides and S^{2-} more effectively. Additionally, Na$^+$ doping widens ion migration channels for Li$^+$, which leads to increased ionic conductivity. Benefiting from the aforementioned triple functions of LNFP, the assembled LSBs exhibit excellent cycling stability at 1 C, along with outstanding kinetic performance even under high sulfur loading and at high current density. This work provides novel insights into the design and fabrication of high-performance cathode additives, offering concrete guidance to facilitate the commercialization of advanced LSBs.

Introduction

The vigorous development of the market is driving researchers to delve deep into the exploration of cutting-edge energy storage devices.[1–5] Among them, the research and development of secondary batteries with high capacity and a long lifespan has become an unstoppable trend. With its exceptional high energy density (2600 Wh kg^{-1}) and outstanding specific capacity (1675 mAh g^{-1}), the lithium–sulfur battery (LSB) precisely aligns with the urgent demands of current market

[a]*Confucius Energy Storage Lab, School of Energy and Environment & Z Energy Storage Center, South East University, Nanjing, Jiangsu, 211189, China*
[b]*School of Mathematics and Physics, University of South China, Hengyang, Hunan, 421001, China*
[c]*State Key Laboratory of Materials-oriented Chemical Engineering & School of Energy Science and Engineering, Nanjing Tech University, Nanjing 211816, China*
† These authors contributed equally to this work.

development.[6-9] However, the active sulfur substances on the cathode side react with lithium ions (Li^+) to form soluble polysulfides during the operation of LSBs. These formed polysulfides freely shuttle between the cathodes and anodes, triggering the so-called 'shuttle effect', which leads to an irreversible loss of active materials. Besides, the inherently limited ionic conductivity of sulfur cathodes makes it difficult for the redox couple of S/S^{2-} especially for thick S cathodes. The above issues significantly constrain the potential of LSBs in practical applications.[10-16] A wide variety of sulfur host materials, encompassing extensive carbon-based materials[17-22] and inorganic compounds,[23-25] are meticulously designed to curb the irreversible loss of active sulfur substances. Regrettably, carbon-based materials inherently exhibit limited anchoring abilities for active substances. Modifying carbon materials, such as grafting active functional groups onto their surfaces, can effectively enhance the anchoring ability of carbon materials toward polysulfides. However, this will inevitably increase the manufacturing cost of the cathode. Due to the inherently poor conductivity and the weak electrochemical activity of the sulfur, relying solely on a tailored sulfur host does not enhance the kinetic performance of redox reactions in LSBs. Furthermore, even if inorganic compounds with special functionalities are prepared for use as sulfur hosts, they still face the issue of escalating production costs. Therefore, constructing a high-performance cathode to enhance the overall performance of LSBs is currently a major technical challenge. Among the various cathode modification strategies, the introduction of functional additives to promote reaction kinetics is recognized as a highly promising and feasible approach.[26-28]

Outstanding ionic conductivity stands as a pivotal characteristic indicator among functional additives, ensuring efficient ion transport. Recent research revealed that lithium salts with certain ionic conductivities such as LTO $(Li_4Ti_5O_{12})$[29] and LFP $(LiFePO_4)$,[30] which combine high stability with environmental friendliness, exhibit potential as modified materials for separators in LSBs. Research reports on the use of such lithium salts as functional additives for cathodes are extremely scarce. To the best of our knowledge, there is still a gap in the research on successfully preparing additives with higher ionic conductivity based on these materials for LSBs. Modifying these materials can further enhance their ionic conductivities. Delving deeper into this field will undoubtedly greatly broaden the selection of additives and open up new avenues for the development of high-performance cathodes. In particular, the adsorption capacity of LFP for polysulfides further confirms its feasibility and application value as an additive for the cathode.[31] LFP can also facilitate the migration of Li^+ cations in LSBs. Furthermore, modifying LFP can further enhance its performance, thereby strengthening its applicability in LSBs. Research findings indicate that incorporating dopant atoms (Zr, Mg, Co, or Na)[32] into LFP is proven to be an effective means of enhancing its ionic conductivity. The performance of doped LFP-based materials in LSBs remains to be thoroughly explored. In addition, micrometer-sized additives reduce the requirements for production equipment compared to nanomaterials in production and practical application, which provides favorable conditions for their large-scale production.

In previous research, we successfully synthesized micrometer-sized $Li_{0.95}Na_{0.05}FePO_4$ (LNFP) and revealed that compared to LFP, LNFP exhibits higher ionic conductivity.[33] Building on this foundation, this work initially validated the practical feasibility of using LNFP as a cathode additive in LSBs. The enhanced ionic conductivity enables effective inward diffusion of polysulfides toward the cathode interior. Specifically, we found that Na^+ doping widens the ion channels of LFP, which implies that LNFP can offer more sites for the adsorption of polysulfides. Meanwhile, Na^+ doping improves the intrinsic electronic conductivity of LFP, thereby enhancing its catalytic conversion ability towards polysulfides. LNFP improves the utilization of active sulfur substances through tri-functionality in ion migration, adsorption, and catalysis. As expected, a LSB employing LNFP as a cathode additive exhibits excellent electrochemical performance. This innovative research provides a valuable reference for the large-scale production of additives. The work carries immense and ground-breaking significance for advancing the commercialization process of high-performance cathodes.

Results and discussion

LNFP particles were prepared *via* a sintering method and subsequently comprehensively characterized. The XRD patterns (Fig. S1) reveal that the diffraction peaks of the prepared LNFP particles are consistent with those of LFP (JCPDS No. 81-1173). This result indicates that the doping of trace amounts of Na atoms does not cause any alteration to the original olivine-type structure of LFP. Through EDS (energy dispersive spectrometer) testing (Fig. S2), sodium elements are found to be uniformly distributed in LNFP. The XPS (X-ray photoelectron spectroscopy) test results also reveal the presence of peaks corresponding to Na (Fig. S3).[34] These results are consistent with our previous findings,[33] indicating the successful preparation of LNFP. Through observation *via* scanning electron microscopy (SEM) images (Fig. S4), it is evident that LNFP exhibits irregular morphological features with dimensions in the micrometer range, which is conducive to large-scale production. It can be seen from the nitrogen adsorption–desorption isotherm that the isotherm of LNFP (Fig. S5a) is similar to that of LFP. The Brunauer–Emmer–Teller (BET) surface area of LNFP is 11 m^2 g^{-1}, which is higher than that of LFP (9 m^2 g^{-1}). This difference is because Na doping widens the ion diffusion channels. The pore size distribution of LNFP is primarily concentrated at around approximately 5 nm (Fig. S5b).

An LNFP/Li cell (the cathode was the LNFP electrode, the anode was lithium foil, and the electrolyte was LS-009) was assembled to validate the feasibility of using LNFP as an additive for the cathode in LSBs. A cyclic voltammetry (CV) test was conducted on the cell at a scan rate of 0.1 mV s^{-1}, and the

results show that no responsive current is generated (Fig. S6a). This indicates that LNFP does not participate in redox reactions independently during the operation of the LSB. Similarly, charge–discharge tests were performed on the cell at 0.13 mA, and no capacity contribution was observed (Fig. S6b). Furthermore, inside an argon-filled glove box, LNFP/Li cells with Li_2S_6 electrolyte (after 50 and 100 cycles) were disassembled. Subsequently, the LNFP electrodes were cleaned and dried. Afterward, these electrodes underwent XRD testing and were compared with an unreacted LNFP electrode. The results reveal an excellent degree of consistency among the XRD diffraction peaks of these three electrodes (Fig. S7). This finding strongly supports the feasibility of the LNFP as a cathode additive.

Aluminum foil coated with LNFP was cut into small circular pieces and assembled as electrodes to form symmetric cells with Li_2S_6 electrolyte, aiming to evaluate the catalytic ability of LNFP towards polysulfides. Additionally, a symmetric cell using the pure electrolyte (LS-009) was assembled as a control for comparative analysis. Through the analysis of CV curves (Fig. S8), it is observed that at a scan rate of 5 mV s^{-1}, the LNFP symmetric cell with the pure electrolyte does not exhibit any noticeable response current. Conversely, the symmetric cell with Li_2S_6 electrolyte demonstrates a significant response current, indicating that the response current originated from the redox reaction of Li_2S_6. Notably, compared to the almost negligible response current of the LFP symmetric cell with Li_2S_6 electrolyte, the LNFP symmetric cell produces a much stronger response current. This finding suggests that Na^+ doping can enhance the catalytic conversion efficiency of LFP towards polysulfides. The reason for this remarkable difference may lie in the fact that the Na^+ doping not only widens the ion diffusion channels in LFP[33] but also alters the electronic environment of Fe^{2+}/Fe^{3+}, thereby improving the intrinsic electronic conductivity of LFP. From the Fe 2p XPS testing results of LFP and LNFP (Fig. S9), it can be observed that there are significant shifts in the peaks corresponding to Fe^{2+} and Fe^{3+} after Na^+ doping, which demonstrates that the introduction of Na alters the electronic environment of Fe^{2+}/Fe^{3+}. It can be observed that the Li_2S nucleation peak current for the C-LNFP electrode appears 14 seconds earlier than that of the C electrode. After the addition of LNFP, the deposition capacity also increases from the original 100 mAh g^{-1} to 147 mAh g^{-1} (Fig. S10). This finding further demonstrates the enhanced electrocatalytic activity of LNFP.[29]

From an experimental perspective, this study aims to reveal the adsorption capacity of LNFP for polysulfides. Based on the same mass of LFP and LNFP, the adsorption capacity of different materials for polysulfides is evaluated by observing the color change of the Li_2S_6 solution. It is found that the Li_2S_6 solution containing LNFP became clear and transparent after 12 h (Fig. S11a), indicating that LNFP has excellent adsorption capacity for polysulfides. From the UV-visible absorption spectra of the corresponding supernatants (Fig. S11b), it can be seen that the absorbance of the LNFP-Li_2S_6 dispersion is weaker than that of the LFP-Li_2S_6 dis-

persion, further proving that LNFP has a stronger adsorption capacity for polysulfides.[35]

To delve deeply into the adsorption mechanism of LNFP towards polysulfides from a theoretical computation perspective, we employed density functional theory (DFT) calculations to analyze the atomic-level interactions between LNFP, LFP, and polysulfides (Fig. 1). Both the LFP and LNFP models are constructed and optimized, respectively. Li_2S_6 as a representative polysulfide is chosen to investigate the adsorption principles by calculating its binding energy with the aforementioned geometric models. Herein, the adsorption energy (E_{ads}) is defined as the total energy when lithium atoms are adsorbed onto the surface, minus the energy of the surface without lithium atom adsorption, further subtracted by the energy of the isolated lithium ion. After calculations, the adsorption energies of different adsorption surfaces on LFP for Li_2S_6 are found to be −2.4 eV, −2.8 eV, and −0.2 eV, respectively. Excitingly, the corresponding adsorption energies on LNFP reach as high as −4.0 eV, −4.3 eV, and −2.1 eV. This result indicates that Na^+ doping leads to a substantial enhancement in the adsorption ability of the functionalized additive toward polysulfides.[36–38] Compared to LFP, LNFP is capable of establishing stronger chemical interactions with polysulfides. When used as a cathode additive, LNFP can more effectively provide active sites for anchoring polysulfides, thereby significantly suppressing the 'shuttle effect'. Both experimental results and theoretical calculations fully demonstrate the promising application prospects of LNFP in LSBs.

The adsorption mechanism of the prepared LNFP towards polysulfides is thoroughly investigated using XPS characterization. After placing equal masses of LFP and LNFP in Li_2S_6 solutions and allowing them to stand for 12 hours, the liquid was removed, and the dried solids were subjected to XPS testing. The trace of sulfate at 169.7 eV is generated due to the exposure of the sample to air (Fig. 2a). Peaks corresponding to polythionate complexes can be observed at 168 eV for both samples (Fig. 2b), indicating that polysulfides can combine with LFP/LNFP to form polythionate complexes, thereby
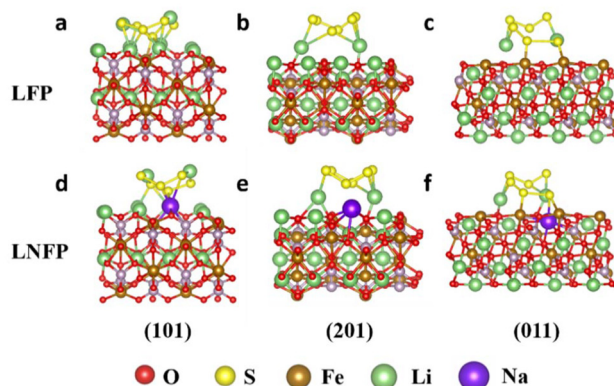

Fig. 1 Theoretical calculations of the adsorption energies of LNFP and LFP for Li_2S_6, key: (a) E_{ads} = −2.4 eV, (b) E_{ads} = −2.8 eV, (c) E_{ads} = −0.2 eV, (d) E_{ads} = −4.0 eV, (e) E_{ads} = −4.3 eV, and (f) E_{ads} = −2.1 eV.

Fig. 2 S 2p XPS spectra of (a) LFP-Li_2S_6, (b) LNFP-Li_2S_6, (c) C–S electrode, and (d) C–S-LNFP electrode (discharged to 1.8 V).

Fig. 3 CV tests. (a) First-cycle CV curves of different cells at 0.1 mV s^{-1}. (b) CV curves of the C–S-LNFP/Li cell at 0.1 mV s^{-1}. (c) CV curves of the C–S-LNFP/Li cell at different scan rates and (d) the corresponding linear matching of peak point currents.

anchoring the polysulfides.[39] Besides, for the Li_2S_6-LNFP sample, a peak belonging to the intermediate product of the thiosulfate can also be detected at 166.7 eV. By combining theoretical calculations, we infer that LFP-based materials can bind with polysulfides to form polythionate complexes. Additionally, Na$^+$ doping widens the diffusion channels in LFP, providing more effective sites for adsorbing polysulfides, resulting in superior polysulfide adsorption of LNFP compared to LFP. After discharging the lithium–sulfur cells to 1.8 V, XPS tests were conducted on the C/S electrode and the C/S electrode doped with LNFP (Fig. 2c and d). Two consistent S 2p peaks are observed, indicating that the adsorbed sulfur substance can be completely desorbed from LNFP during the redox reaction process.

Cathodes doped with LFP and LNFP were prepared separately, and for comparison, an undoped cathode was also prepared. These cathodes are sequentially labeled as C–S-LFP, C–S-LNFP, and C–S. Subsequently, different cathodes are assembled into lithium–sulfur cells to evaluate the practical effects of various additives in applications. Different assembled cells were subjected to CV testing. The results indicate that the cell with the LNFP additive exhibits CV curves with a large peak area and narrow distance between oxidation and reduction peaks at 0.1 mV s^{-1} (Fig. 3a). This characteristic suggests that the oxidation–reduction reactions in the C–S-LNFP/Li cells proceed fully, with weak polarization phenomena.[40] Besides, compared to the C–S/Li and C–S-LFP/Li cells, the C–S-LNFP/Li cells demonstrate excellent overlap in their first three CV curves (Fig. 3b and S12), strongly evidencing that LNFP can enhance the kinetic process of oxidation–reduction reactions.

At various scanning rates, the CV characteristics of different cells were tested. The observation results indicate that even when the scanning rate is increased to 0.5 mV s^{-1}, the C–S-LNFP/Li cell still exhibits distinguishable oxidation–reduction peaks (Fig. 3c, S13a, and S13b). By utilizing linear
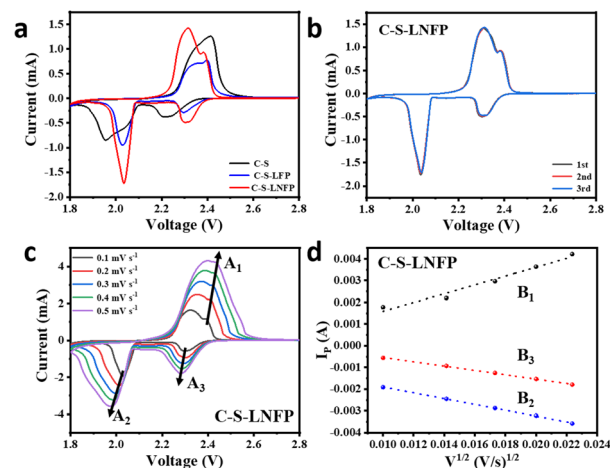
matching (Fig. 3d, S13c, and S13d), the Li$^+$ diffusion coefficients of different batteries under various voltage conditions were calculated. Upon comparative analysis, it is found that the Li$^+$ diffusion coefficient of the C–S-LNFP/Li cell is higher than that of the C–S/Li and C–S-LFP/Li cells (Table S1). This advantage is attributed to the enhanced ionic conductivity of LNFP, which facilitates the rapid migration of Li$^+$ cations.

After 100 cycles at 1 C, different lithium–sulfur cells were subjected to electrochemical impedance spectroscopy (EIS) tests (Fig. S14). Following these cycles, the C–S-LNFP/Li cell exhibits a reduced bulk resistance (R_S) in comparison with both the C–S/Li and C–S-LFP/Li cells (Table S2). This indicates that LNFP as a cathode additive can provide more active reaction sites, which enhances the interaction between the electrolyte and sulfur. Notably, the interfacial resistance (R_{SEI}) of the C–S-LNFP/Li cell is the lowest among the three, suggesting the formation of a more stable SEI (solid electrolyte interface) film during cycling.[41] This phenomenon can likely be attributed to the strong physical adsorption ability of LNFP for polysulfides, mitigating corrosion of the lithium anode. It is worth noting that the C–S-LNFP/Li cell also displays a low charge transfer resistance (R_{CT}), an advantage that stems from the inherent excellent ionic conductivity of LNFP.[42] The low charge transfer resistance of the C–S-LNFP/Li cell also strongly demonstrates that Na doping enhances the intrinsic electronic conductivity of LFP.

At 1 C, the initial discharge specific capacities of C–S/Li, C–S-LFP/Li, and C–S-LNFP/Li cells are found to be 785 mAh g^{-1}, 766 mAh g^{-1}, and 953 mAh g^{-1}, respectively (Fig. 4a). Among them, the C–S-LNFP cell exhibits a superior initial discharge specific capacity, surpassing the other two cells. This performance strongly demonstrates its efficient utilization of active sulfur substances. After 700 cycles, the capacity decay rates per cycle for these three cells are controlled at 0.084%, 0.059%, and a lower 0.039%, respectively. It is gratifying that the dis-
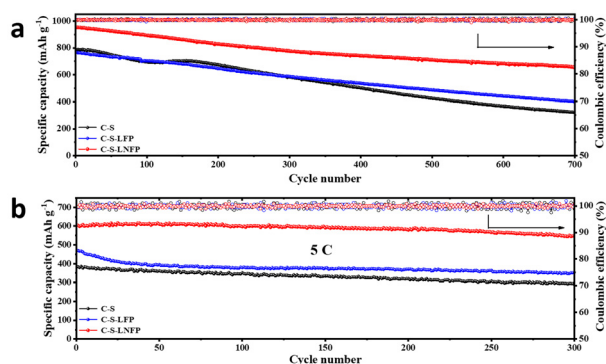
Fig. 4 The cycling performances of different cells at (a) 1 C and (b) 5 C.

charge specific capacity of the C–S-LNFP/Li cell still reaches 652 mAh g^{-1} after prolonged cycling. The exceptional cycling performance of the C–S-LNFP/Li cell underscores the multiple roles of LNFP as a cathode additive: it not only suppresses the 'shuttle effect' but also enhances the kinetics of redox reactions. By analyzing the corresponding charge/discharge curves (Fig. S15), it can be observed that the discharge specific capacities of the C–S/Li and C–S-LFP/Li cells exhibit a relatively rapid decay trend. In contrast, the capacity of the C–S-LNFP/Li cell demonstrates remarkably stable retention. Compared to the other two cells, the C–S-LNFP/Li cell delivers superior specific discharge capacities across various current density conditions (Fig. S16). This performance strongly evidences that Na$^+$ doping in LFP can enhance the rate ability of the cathode. Furthermore, the C–S-LNFP/Li cell exhibits distinctly visible charge/discharge curves at different current densities, highlighting the notable advantages of LNFP in LSBs.[43–45] Compared to similar studies, this project demonstrates remarkable competitiveness (Table S3), convincingly showcasing the immense potential and value of LNFP as a high-performance sulfur cathode additive for commercial use.

The key challenge for the commercialization of LSBs lies in achieving good cycling stability under high sulfur loading and high current density conditions. Therefore, it is indispensable to conduct cycling performance tests on LSBs under such harsh conditions. At 5 C, the initial discharge specific capacities of C–S/Li, C–S-LFP/Li, and C–S-LNFP/Li cells are 384, 470, and 604 mAh g^{-1}, respectively (Fig. 4b). Particularly noteworthy is that even under such demanding current density, the C–S-LNFP/Li cell can maintain a high discharge specific capacity, an achievement largely attributed to the excellent ion conductivity of LNFP itself. As expected, the C–S-LNFP/Li cell still retains a discharge specific capacity of 548 mAh g^{-1} after 300 cycles at 5 C, and this remarkable cycling stability performance is likely due to the inherent high stability of LNFP. These results strongly demonstrate the superiority of Na$^+$ doping.

High sulfur loading cathodes were prepared, with the additive content maintained consistent with that in conventional sulfur loading cathodes. Subsequently, the assembled cells underwent cycling performance evaluations (Fig. S17). Unlike

the cathode without any additives, which exhibits low discharge specific capacities (only 320 mAh g^{-1}), the cathode with added LNFP demonstrates higher discharge specific capacities (~880 mAh g^{-1}) under high sulfur loading conditions (4.5 mg cm^{-2}). This finding robustly confirms that even under harsh high sulfur loading conditions, LNFP can also promote the redox reaction kinetics within the battery, thereby highlighting its vast application prospects and tremendous potential as a commercial sulfur cathode additive. A lithium–sulfur pouch cell incorporating the LNFP additive in the cathode was fabricated to evaluate its electrochemical performance.[46–48] It shows a stable open circuit voltage of 2.96 V (Fig. S18a) and can power light emitting-diode lamps (Fig. S18b) showing the capital letters of blurred 'SEU'.

After 100 cycles at 1 C, the cells were disassembled in an argon-filled glove box, and the cathodes were subjected to SEM testing. For direct comparison, the cathodes before cycling were also tested using SEM. The observation results indicated that the cathodes before cycling all exhibit a loose and porous structure (Fig. 5a–c). However, the dense layers composed of deposited sulfur substances with lower electrochemical activity formed notably on the surfaces of the cycled C–S (Fig. 5d) and C–S-LFP (Fig. 5e) cathodes. The presence of these dense layers hinders the full utilization of active sulfur substances. In contrast, the cycled C–S-LNFP cathode retains a loose and porous structure (Fig. 5f) owing to the rapid ion transport channels enabled by LNFP, a feature that promotes deep polysulfide penetration and diffusion.[49] This result intuitively highlights the advantages of LNFP in the applications of LSBs.

With the aid of schematic illustrations, this paper visually demonstrates the notable advantages of LNFP in LSB applications. In the absence of any functional cathode additives (Fig. 6a), the prepared LSBs generate soluble polysulfides during operation, which can easily penetrate the separator, leading to irreversible loss of active materials and accelerated corrosion of the lithium anode. This phenomenon poses a serious threat to the service life and safety of LSBs, greatly hindering their commercialization process. In contrast, when
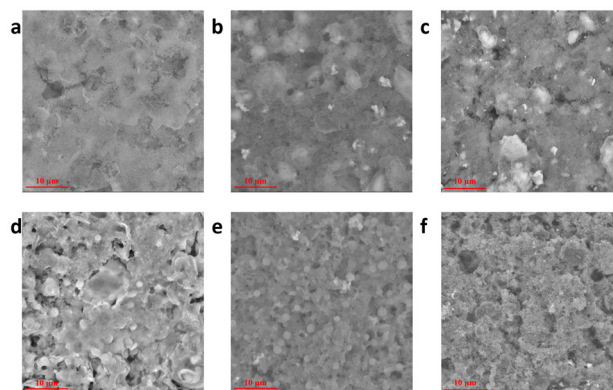

Fig. 5 SEM of cathodes: (a) C–S, (b) C–S-LFP, and (c) C–S-LNFP before cycling and (d–f) the corresponding cathodes after cycling (1 C, 100 cycles).
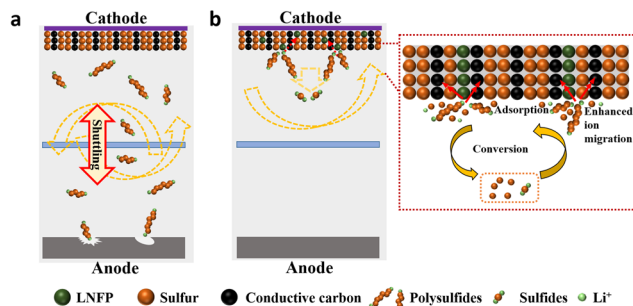
Fig. 6 Schematic diagrams of actions of the (a) C–S and (b) C–S-LNFP cathodes in LSBs (inset: partial enlargement).

LNFP is used as a functional additive for the cathode, its exceptional adsorption ability for sulfur substances anchors the generated polysulfides, preventing their unrestricted diffusion (Fig. 6b). Simultaneously, LNFP can accelerate the catalytic conversion of soluble polysulfides into insoluble sulfides, ensuring efficient utilization of active sulfur substances. The enhanced ionic conductivity of LNFP additionally ensures efficient ion transport, facilitating polysulfide diffusion within the cathode. The multifunctional effects of LNFP contribute to a high-performance sulfur cathode.

Conclusions

In summary, micrometer-sized LNFP was successfully synthesized. We find that the prepared LNFP can effectively adsorb polysulfides due to the wide ion channels caused by Na^+ doping. Additionally, Na^+ doping alters the electronic environment of Fe^{2+}/Fe^{3+}, which improves the intrinsic electronic conductivity of LFP. Na^+ doping also accelerates Li^+ diffusion, leading to improved ionic transport kinetics. Through theoretical calculations and experimental verification, the practical feasibility of LNFP as a functional additive for the cathode of LSBs is confirmed. A LSB using LNFP as an additive exhibits a capacity decay rate of only 0.039% per cycle after 700 cycles at 1 C. Even at a high current density of 5 C, the assembled LSB can stably cycle 300 times while maintaining a discharge specific capacity of approximately 600 mAh g^{-1}. After cycling, no accumulation of non-conductive sulfur substances is observed on the surface of the cathode. This groundbreaking research addresses the current limitation of lithium salts as cathode additives with limited ionic conductivity and simultaneously broadens the selection scope of functional additive materials for cathodes, holding profound implications for the future commercialization of advanced LSBs.

Experimental section

Preparation of LFP and LNFP

The preparation of LNFP is similar to that in previous reports.[33] Briefly, Na_2CO_3, $NH_4H_2PO_4$, $FeC_2O_4\cdot2H_2O$, and Li_2CO_3 are meticulously measured and placed in an agate bowl based on their stoichiometric proportions. The ensuing mixture undergoes ball milling at a speed of 400 rpm for 10 hours. Subsequently, the mixture is subjected to a thermal treatment process under the protective atmosphere of argon. The heated product is subjected to ball milling once again to obtain the desired LNFP powder. LFP is prepared using the same method for comparison, except that Na_2CO_3 is not added.

Preparation of conventional sulfur loading cathodes

First, acidified carbon nanotubes (CNTs) and sublimed sulfur are mixed uniformly at a mass ratio of 3 : 7. Subsequently, this mixture is placed in a Teflon liner filled with argon gas. Then, the liner is placed inside a reaction kettle, which is then positioned within a muffle furnace (155 °C, 12 h). After the temperature in the muffle furnace naturally drops to room temperature, the reaction kettle is removed. Finally, the retrieved sample is ground, yielding a carbon–sulfur (C–S) composite material.

The C–S composite, PVDF (polyvinylidene difluoride), and conductive carbon, with a mass ratio of 8 : 1 : 1, are placed in a small beaker. An appropriate amount of NMP (N-methylpyrrolidone) is then added, and the mixture is magnetically stirred until a homogeneous slurry is formed. Subsequently, this slurry is poured onto the surface of aluminum foil and spread evenly. After undergoing vacuum drying overnight, the aluminum foil coated with the slurry is cut into small circular discs with a diameter of 10 mm, thus successfully obtaining the C–S cathodes. The preparation process for the C–S-LFP and C–S-LNFP cathodes is similar to that of the C–S cathode. In both cases, the content of LFP ($LiFePO_4$) and LNFP in the cathode materials is controlled at 5 wt%. The sulfur loading is approximately 1.0 mg cm^{-2}.

Preparation of high sulfur loading cathodes

High sulfur loading cathodes (4.5 mg cm^{-2}) are prepared according to the previous report.[6] The carbon–sulfur composite, CMC (carboxymethyl cellulose), and conductive carbon (the mass ratio is 7 : 1 : 1) are added to deionized water containing dissolved CMC. The mixture is stirred until forming a homogeneous slurry. This slurry is coated onto carbon-coated aluminum foil. Then, the aluminum foil loaded with different materials is vacuum-dried overnight and cut into small circular discs to obtain high-loading cathodes. The preparation of C–S-LFP and C–S-LNFP high sulfur loading cathodes follows the same procedure as that for the C–S cathode, except that LFP and LNFP are added to the slurry, respectively. The content of functional additives in the high sulfur loading cathodes is controlled to be the same as that in conventional sulfur loading cathodes.

Assembly of coin-type cells

A sulfur cathode, a separator, and a lithium metal anode are sequentially encapsulated inside a CR2025 coin shell in an argon-filled glove box (O_2 < 0.1 ppm, H_2O < 0.1 ppm). After

being compacted under a certain pressure, a lithium–sulfur cell is obtained. The electrolyte (LS-009) is dripped onto both sides of the separator, with the electrolyte quantity precisely controlled for each cell (40 μL). The prepared lithium–sulfur cells are labeled as C–S/Li, C–S-LFP/Li, and C–S-LNFP/Li cells, respectively, based on the different cathodes used.

As for testing the catalytic performance of LNFP towards polysulfides. The assembly process for the Li_2S_6 symmetric cell is similar to that of the lithium–sulfur cell, with both the cathode and anode being the LNFP electrodes. The Li_2S_6 electrolyte is dripped onto both sides of the separator. In addition, a pure LS-009 symmetric cell is prepared for comparison.

Conflicts of interest

There are no conflicts of interest to declare.

Data availability

The data supporting this article have been included as part of the supplementary information (SI). Supplementary information is available. See DOI: https://doi.org/10.1039/d5eb00160a.

Acknowledgements

References

1 Z. Fan, Y. Li, J. Pan, Z. Zhou, W. Li, T. Yang, H. Zhang, C. Shu, W. Hua, Y. Wu and W. Tang, *EES Batteries*, 2025, **1**, 100–118.

2 C. Wu, Z. Wang, Z. Jia, J. Cui, C. Shu, X. Wang, Y. Wu and W. Tang, *EES Batteries*, 2025, **1**, 364–384.

3 H. Liu, X. Liu, W. Li, X. Guo, Y. Wang, G. Wang and D. Zhao, *Adv. Energy Mater.*, 2017, **7**, 1700283.

4 J. Guo, J. Huo, Y. Liu, W. Wu, Y. Wang, M. Wu, H. Liu and G. Wang, *Small Methods*, 2019, **3**, 1900159.

5 S. Zheng, H. Geng, S. N. Eliseeva and B. Wang, *Energy Mater.*, 2022, **2**, 200042.

6 S. Xia, Z. Lin, B. Peng, X. Yuan, J. Du, X. Yuan, L. L. Liu, L. J. Fu, R. Holze and Y. P. Wu, *Energy Environ. Sci.*, 2024, **17**, 5461.

7 T. Wang, J. He, X.-B. Cheng, J. Zhu, B. Lu and Y. Wu, *ACS Energy Lett.*, 2022, **8**, 116–150.

8 S. Xia, X. Xu, W. Wu, Y. Chen, L. Liu, G. Wang, L. Fu, Q. Zhang, T. Wang, J. He and Y. P. Wu, *Mater. Sci. Eng., R*, 2025, **163**, 100924.

9 J. Song, S. Xia, N. Wang, J. Peng, B. Peng, W. Wu, L. Liu, X. Yuan, L. Fu, Y. Chen and Y. P. Wu, *Adv. Mater.*, 2024, **37**, 2418295.

10 H. Song, K. Münch, X. Liu, K. Shen, R. Zhang, T. Weintraut, Y. Yusim, D. Jiang, X. Hong, J. Meng, Y. Liu, M. He, Y. Li, P. Henkel, T. Brezesinski, J. Janek and Q. Pang, *Nature*, 2025, **637**, 846–853.

11 X. Pang, H. Geng, S. Dong, B. An, S. Zheng and B. Wang, *Small*, 2022, **19**, 2205525.

12 J. Li, Z. Wang, K. Shi, Y. Wu, W. Huang, Y. Min, Q. Liu and Z. Liang, *Adv. Energy Mater.*, 2023, **14**, 2303546.

13 Q. Chen, J. Li, J. Pan, T. Li, K. Wang, X. Li, K. Shi, Y. Min and Q. Liu, *Small*, 2024, **20**, 2401153.

14 K. Li, T. Li, Z. Wang, K. Shi, Y. Sun, J. Li, J. Ren, A. Lu, X. Li and Q. Liu, *Adv. Funct. Mater.*, 2024, **34**, 2410517.

15 Z. Wang, W. Huang, H. Wu, Y. Wu, K. Shi, J. Li, W. Zhang and Q. Liu, *Adv. Funct. Mater.*, 2024, **34**, 2409303.

16 T. Li, K. Shi, X. Li, W. Huang, J. Li, J. Li, K. Wang, Y. Deng, H. Chen, Y. Min, J. Li and Q. Liu, *Adv. Funct. Mater.*, 2025, 2505615.

17 X. Cui, X. Wang and Q. Pan, *Energy Mater.*, 2023, **3**, 300034.

18 S. Shen, L. Huang, X. Tong, R. Zhou, Y. Zhong, Q. Xiong, L. Zhang, X. Wang, X. Xia and J. Tu, *Adv. Mater.*, 2021, **33**, 2102796.

19 P. Han, S. H. Chung and A. Manthiram, *Small*, 2019, **15**, 1900690.

20 Z. Luo, W. Lei, X. Wang, J. Pan, Y. Pan and S. Xia, *J. Alloys Compd.*, 2020, **812**, 152132.

21 Z. Luo, X. Wang, W. Lei, P. Xia and Y. Pan, *J. Mater. Sci. Technol.*, 2020, **55**, 159–166.

22 P. Zhu, J. Zhu, C. Yan, M. Dirican, J. Zang, H. Jia, Y. Li, Y. Kiyak, H. Tan and X. Zhang, *Adv. Mater. Interfaces*, 2018, **5**, 1701598.

23 H. M. Kim, J.-Y. Hwang, S. Bang, H. Kim, M. H. Alfaruqi, J. Kim, C. S. Yoon and Y.-K. Sun, *ACS Energy Lett.*, 2020, **5**, 3168–3175.

24 H.-E. Wang, K. Yin, N. Qin, X. Zhao, F.-J. Xia, Z.-Y. Hu, G. Guo, G. Cao and W. Zhang, *J. Mater. Chem. A*, 2019, **7**, 10346–10353.

25 H. Lee, H. Nam and J. H. Moon, *Energy Storage Mater.*, 2024, **70**, 103551.

26 N. Li, T. Meng, L. Ma, H. Zhang, J. Yao, M. Xu, C. M. Li and J. Jiang, *Nano-Micro Lett.*, 2020, **12**, 145.

27 K. Sun, M. Fu, Z. Xie, D. Su, H. Zhong, J. Bai, E. Dooryhee and H. Gan, *Electrochim. Acta*, 2018, **292**, 779–788.

28 M. Zheng, X. Gao, Y. Sun, K. Adair, M. Li, J. Liang, X. Li, J. Liang, S. Deng, X. Yang, Q. Sun, Y. Hu, Q. Xiao, R. Li and X. Sun, *Small Methods*, 2021, **5**, 2100176.

29 S. Xia, J. Song, Q. Zhou, L. L. Liu, J. L. Ye, T. Wang, Y. H. Chen, Y. K. Liu, Y. P. Wu and T. Ree, *Adv. Sci.*, 2023, **10**, 2301386.

30 S. Xia, Z. Chen, L. Yuan, J. Song, Q. Zhou, X. Yuan, L. Liu, L. Fu, Y. Chen and Y. Wu, *J. Mater. Chem. A*, 2023, **11**, 19870–19876.

31 X. Gao, C. Zheng, Y. Shao, V. R. Shah, S. Jin, J. Suntivich and Y. L. Joo, *ACS Appl. Mater. Interfaces*, 2023, **15**, 19011–19020.

32 S.-P. Chen, D. Lv, J. Chen, Y.-H. Zhang and F.-N. Shi, *Energy Fuels*, 2022, **36**, 1232–1251.

33 B. Peng, Z. Liu, Q. Zhou, X. Xiong, S. Xia, X. Yuan, F. Wang, K. I. Ozoemena, L. Liu, L. Fu and Y. P. Wu, *Adv. Mater.*, 2023, **36**, 2307142.

34 E. M. Lotfabad, J. Ding, K. Cui, A. Kohandehghan, W. P. Kalisvaart, M. Hazelton and D. Mitlin, *ACS Nano*, 2014, **8**, 7115–7129.

35 C. Barchasz, F. Molton, C. Duboc, J. C. Lepretre, S. Patoux and F. Alloin, *Anal. Chem.*, 2012, **84**, 3973–3980.

36 Q. Liang, S. Wang, X. Lu, X. Jia, J. Yang, F. Liang, Q. Xie, C. Yang, J. Qian, H. Song and R. Chen, *ACS Nano*, 2024, **18**, 2395–2408.

37 C. Shang, L. Cao, M. Yang, Z. Wang, M. Li, G. Zhou, X. Wang and Z. Lu, *Energy Storage Mater.*, 2019, **18**, 375–381.

38 J. Xu, S. An, X. Song, Y. Cao, N. Wang, X. Qiu, Y. Zhang, J. Chen, X. Duan, J. Huang, W. Li and Y. Wang, *Adv. Mater.*, 2021, **33**, 2105178.

39 X. Liang, C. Hart, Q. Pang, A. Garsuch, T. Weiss and L. F. Nazar, *Nat. Commun.*, 2015, **6**, 5682.

40 E. Jing, L. Chen, S. Xu, W. Tian, D. Zhang, N. Wang, Z. Bai, X. Zhou, S. Liu, D. Duan and X. Qiu, *J. Energy Chem.*, 2022, **64**, 574–582.

41 D. Yang, L. He, Y. Liu, W. Yan, S. Liang, Y. Zhu, L. Fu, Y. Chen and Y. Wu, *J. Mater. Chem. A*, 2019, **7**, 13679–13686.

42 A. Zhang, X. Fang, C. Shen, Y. Liu, I. G. Seo, Y. Ma, L. Chen, P. Cottingham and C. Zhou, *Nano Res.*, 2018, **11**, 3340–3352.

43 J. Zhou, C. Shu, J. Cui, C. Peng, Y. Liu, W. Hua, L. Simonelli, Y. Wu, S. X. Dou and W. Tang, *Carbon Energy*, 2024, **6**, e460.

44 Y. Ding, T. Yan, J. Wu, M. Tian, M. Lu, C. Xu, J. Gu, H. Zhao, Y. Wang, X. Pan, S. X. Dou, L. Zhang and J. Sun, *Appl. Catal., B*, 2024, **343**, 123553.

45 Q. Lv, Y. Sun, B. Li, C. Li, Q. Zhang and L. Wang, *Adv. Energy Mater.*, 2025, **15**, 2403223.

46 Y. Song, X. Long, Z. Luo, C. Guo, C.-N. Geng, Q.-S. Ouyang, Z. Han, G. Zhou and J.-J. Shao, *ACS Appl. Mater. Interfaces*, 2022, **14**, 32183–32195.

47 Y. Song, H. Li, J. Li, J. An, J.-J. Shao and G. Zhou, *J. Energy Chem.*, 2023, **87**, 51–60.

48 Y. Song, M. Zhou, Z. Chen, H. Nie, J.-J. Shao and G. Zhou, *Chin. Chem. Lett.*, 2024, **35**, 109200.

49 H. Yao, K. Yan, W. Li, G. Zheng, D. Kong, Z. W. Seh, V. K. Narasimhan, Z. Liang and Y. Cui, *Energy Environ. Sci.*, 2014, **7**, 3381–3390.